Electric field induced effects in Y3N@[C80]6-anionic solid

Electric field induced effects in Y3N@[C80]6− anionic solid

Yong Sun, Hiroki Sezaimaru, Masamichi Sakaino, Naoto Ogawa, and Kenta Kirimoto

Citation: Journal of Applied Physics **117**, 154308 (2015); doi: 10.1063/1.4918665
View online: http://dx.doi.org/10.1063/1.4918665
View Table of Contents: http://scitation.aip.org/content/aip/journal/jap/117/15?ver=pdfcov
Published by the AIP Publishing

Electric field induced effects in $Y_3N@[C_{80}]^{6-}$ anionic solid

Yong Sun,[1,a)] Hiroki Sezaimaru,[1] Masamichi Sakaino,[1] Naoto Ogawa,[2] and Kenta Kirimoto[2]
[1]*Department of Applied Science for Integrated System Engineering, Kyushu Institute of Technology, Senshuimachi, Tobata, Kitakyushu, Fukuoka 804-8550, Japan*
[2]*Department of Electrical and Electronic Engineering, Kitakyushu National College of Technology, 5-20-1 shii, Kokuraminami, Kitakyushu, Fukuoka 802-0985, Japan*

(Received 3 October 2014; accepted 9 April 2015; published online 21 April 2015)

By measuring the $i - v$ characteristics of $Y_3N@[C_{80}]^{6-}$ anionic solid at various temperatures and electric field strengths, four conducting phases with $i \propto v$, $i \propto v^2$ with low resistance, $i \propto v^4$ and $i \propto v^2$ with high resistance were observed. First, at temperatures below 100 K and field strengths below 30 Vcm^{-1}, the current passing through the sample was a linear function of the d.c. bias voltage due to free moving charges. Second, at the same field strengths, the trapped carrier was thermally activated with activation energies of 13.6 meV for temperature range of 100 – 250 K and 88.7 meV for 250 – 450 K. In this conducting phase, the carrier transport was governed by space charge limited conduction mechanism. Third, when the electric field increased from 30 to 120 Vcm^{-1}, the i became a quartic function of the v because the carrier mobility is a quadratic function of the field strength. A conducting phase with high resistance was observed at temperatures below 100 K. The trapped carrier was thermally activated with activation energies of 146.5 meV for temperature range of 100 – 250 K and 288.5 meV for 250 – 450 K. Finally, in the electric field strengths of 120 – 2000 Vcm^{-1}, a high resistance phase appeared in the anionic solid at temperatures below 100 K. The current was a quadratic function of the d.c. bias voltage, and the carrier mobility was independent of the field strength.
[http://dx.doi.org/10.1063/1.4918665]

I. INTRODUCTION

Trimetallic nitride endohedral fullerenes, M_3N cluster encapsulated in C_{2n} carbon cage, have attracted increasing attentions for their potential applications in electronics,[1] magnetics,[2] photonics,[3] and bio-technology.[4] Many studies have been carried out for interactions between the cluster and the carbon cage. The charge transfer from the cluster to the carbon cage has been widely investigated,[5–9] as these materials are expected to display remarkable electronic and structural properties associated with this charge transfer.[10–12] Dipole polarizability of the $M_3N@C_{2n}$ fullerenes have been studied by using density functional theory (DFT).[13–15] Unlike nonmetal endohedral fullerenes, $M_3N@C_{2n}$ show smaller dipole polarizability than the corresponding C_{2n} empty cage because the induced electric field of the carbon cage is reduced by inserting the M_3N cluster. Functionalization of $Sc_3N@C_{80}$ has been accomplished using both a Diels-Alder reaction and an azomethine ylide addition.[16,17] In the case of Diels-Alder reaction, addition products were formed at the 5:6 ring junction of the C_{80} cage. On the other hand, azomethine ylide addition to $Y_3N@C_{80}$ produced an adduct at the 6:6 ring junction.[18,19] Namely, the internal metal ions appear to exert control over the site of addition. While molecular properties of the $M_3N@C_{80}$ fullerenes have been reported, to best of our knowledge, the electronic interactions between the $M_3N@C_{80}$ molecules or between the M_3N clusters in crystalline phase are not still studied.

The Y atoms are the formal 3+ oxidation state in $Y_3N@C_{80}$ molecule. Three and six electrons from the Y atom transferred to the N atom and the C_{80} cage. NMR investigations of the nuclei of Y_3N cluster revealed that the pentalene group strongly binds to one yttrium atom and prevents the cluster rotation, whereas in $Y_3N@C_{80}$ molecule the cluster undergoes nearly free isotropic rotation.[20] Moreover, Dorn *et al*. have suggested that the rotation energetic barriers of the Y_3N cluster is dependent on the ionic radius of the Y^{3+} ions.[21] The Y_3N cluster is slightly pyramidal inside the C_{80} cage[22] and cannot rotate freely as planar M_3N, such as Sc_3N, Lu_3N, and Er_3N, does inside the cage. Recently, we have studied the carrier transport properties of $Sc_3N@C_{80}$,[23] $Lu_3N@C_{80}$,[24,25] and $Er_3N@C_{80}$[26] by measuring the current-voltage (i-v) characteristics. No significant temperature and electric field effects have be observed on those $M_3N@C_{80}$ molecules because of small diameters of the endohedral clusters.

In this study, we characterized carrier transport properties of the $Y_3N@[C_{80}]^{6-}$ anionic solid at various temperatures and electric field strengths. The i-v characteristics in this study showed that there is an interaction between the ionized Y_3N clusters through the carbon cages in crystalline phase. The interaction depends on both temperature and the applied electric field. At temperatures above 100 K, charge carriers in the $Y_3N@[C_{80}]^{6-}$ anionic solid were thermally activated with various activation energies as well as the i-v characteristics were a quadratic function for low fields and a

[a)]E-mail: sun@ele.kyutech.ac.jp

quartic function for high fields. On the other hand, at temperatures below 100 K, the *i-v* characteristics were a linear function for low fields and a quartic function for high fields. Under high electric fields, molecular interactions change its potential and result in an order phase transition of theY_3N clusters in the C_{80} cages in broad temperature range from 15 to 450 K.

II. EXPERIMENTAL

$Y_3N@C_{80}$ powder with purity >97 wt. % was purchased from LUNA Innovations to make a sample specimen for measurement. The $Y_3N@[C_{80}]^{6-}$ powder was pressed into a pellet at room temperature at 1.25 GPa for 50 min. The so formed pellet was 5.0 mm in diameter and 0.50 mm in thickness. Two gold electrodes on the surfaces of the sample were prepared using an Au nano-particle paste (NAU-K05B, Daiken), and the sample was annealed at temperature of 450 K in vacuum for 30 min in order to degas for the sample as well as to reduce the gold as the electrodes. Prior to electrical measurements, the samples were characterized by x-ray photoemission spectroscopy (XPS, AXIS-NOVA, SHIMATSU/KRATOS) and x-ray diffraction (XRD, JEOL JDX-3500 K). In the XPS analysis, the beam diameter of Al Kα line was 55 μm, and the binding energy resolution was 0.15 eV.

In the measurements, the current passing through the sample was measured using a digital electrometer (ADVANTEST R8252) with a current resolution of 1.0 fA at various d.c. bias voltages from 0.001 V to 100.0 V. The pellet sample was set in a vacuum chamber of a cryostat during the measurements. The base pressure of the vacuum chamber was less than 10^{-5} Pa. The current measurements were carried out in the course of heating up or cooling down process between the temperatures from 15 K to 450 K. The rate of heating or cooling was 0.14 K min^{-1} with a stepwise increment of 1.0 K.

The a.c. impedance $Z = Z' + jZ''$ of the sample was measured at room temperature in atmosphere to characterize contact resistance between the electrode and the sample by using a Cole-Cole plot method. The Cole-Cole plot was drawn using the imaginary part $-Z'' = -\mathrm{Im}[Z]$ and the real part $Z' = \mathrm{Re}[Z]$.

III. RESULTS AND DISCUSSION

Typical x-ray photoemission spectrum of the pellet sample at room temperature was show in Fig. 1. It was obtained from the surface of the $Y_3N@[C_{80}]^{6-}$ sample after Ar^+ ion sputtering for 25 s. Eight peaks at binding energies of 24, 45, 156, 285, 299, 311, 394, 531, and 990 eV were observed in the spectrum. The 24 and 45 eV peaks are attributed to photoemissions from 4*p* and 4*s* electrons of Y atoms. The double peaks at 156 and 158 eV were photoemissions from Y $3d^{5/2}$ and Y $3d^{3/2}$. The peaks at 299, 311, and 394 eV were related to photoemissions from $3p^{3/2}$, $3p^{1/2}$, and 3*s* electrons of Y atoms. The peak around 285 and 531 eV comes from C 1*s* and O 1*s* core level, respectively. The peak around 990 eV corresponds to O KLL Auger electron emission.

The enlarged photoemission spectra from O 1*s* core level at binding energy of 531 eV were shown in Fig. 2(a) for various Ar^+ ion sputtering times of 0, 5, 15, and 25 s. The Ar^+ ion sputtering results in both the decrease in the peak intensity and the peak shift toward low energy side. The oxygen atoms adsorbed only on the surface of the pellet sample because both intensity and position of the peak do not change when the Ar^+ ion sputtering time is above 15 s.

Figure 2(b) shows the photoemission spectra from C 1*s* core level at binding energy of 285 eV for various Ar^+ ion sputtering times of 0, 5, 15, and 25 s. No significant changes on both intensity and position of the peak were observed after the Ar^+ ion sputtering. The result suggests an oxygen adsorption molecular or small amount on the surface of the sample.

The double peaks from Y $3d^{5/2}$ and $3d^{3/2}$ core levels of Y atoms were plotted in Fig. 2(c) in the enlarged energy scaling. The positions of the double peaks are observed at 158 and 160 eV, which shifted toward high energy side as compared with theoretical values of 156 and 158 eV. This may be due to a screening from the C_{80} carbon cage. The peak intensity increases but its position does not change with increasing Ar^+ ion sputtering time. This result suggests that there is not direct electronic interaction between the Y atoms with the oxygen atoms adsorbed on the surface of the C_{80} cage. On the other hand, desorption of the oxygen atoms from the surface of the C_{80} cage results in larger photoemission from the Y atoms. From the spectrum after the Ar^+ ion sputtering of 25 s, atomic ratio of Y/C is evaluated to be 3.47 at. %, which closes to stoichiometric ratio of 3.75 at. % for $Y_3N@C_{80}$. Also, the photoemission from N atoms cannot be detected due to its smaller relative sensitivity factor (RSF, 0.505) and concentration as well as the screening of the C_{80} cage.

XRD pattern of the $Y_3N@[C_{80}]^{6-}$ powder was shown in Fig. 3. Few diffraction peaks can be recognized for the pattern, a strong peak at $2\theta = 9.30°$ and two broad peaks centered at $2\theta = 17.9$ and 24.95°. For comparison, the XRD

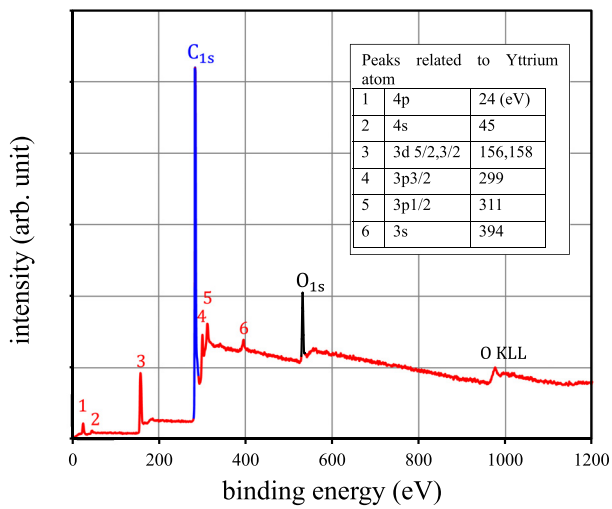

FIG. 1. X-ray photoemission spectra of the $Y_3N@[C_{80}]^{6-}$ anionic solid prepared at a pressure of 1.25 GPa. The spectrum was detected on the surface of the sample after Ar^+ ion sputtering for 25 s.

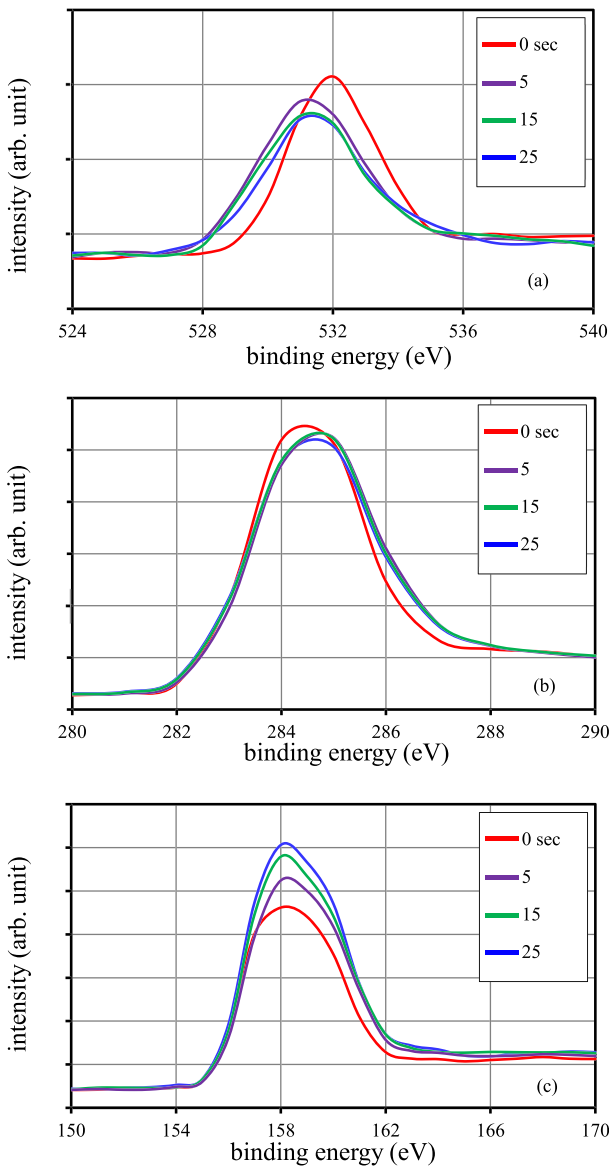

FIG. 2. (a) Enlarged x-ray photoemission spectra from O 1*s* core level before and after Ar^+ ion sputtering for 5, 15, and 25 s, (b) the spectra from C 1*s* core level before and after Ar^+ ion sputtering for 5, 15, and 25 s, and (c) the spectra from Y $3d^{5/2}$ and $3d^{3/2}$ core levels before and after Ar^+ ion sputtering for 5, 15, and 25 s.

pattern of C_{60} powder was also shown in this figure. The $2\theta = 9.30$ peak was ascribed to the diffraction from (111) planes of a face-centered cubic (fcc) crystal structure with a lattice constant of 1.61 nm. Other two broad peaks are related to overlapped diffraction results from several crystal planes. The peak at $2\theta = 17.9$ corresponds to (220), (311), and (222) planes and the peak at $2\theta = 24.95$ is related to diffractions from (331), (420), (422), and (511) planes. The grain size of the $Y_3N@[C_{80}]^{6-}$ powder was estimated to be 7.6 nm from full width at half-maximum (FWHM) of the (111) peak.

Cole–Cole plots of the a.c. impedance of the Au/$Y_3N@[C_{80}]^{6-}$/Au structure at room temperature at amplitudes of 0.05, 0.5, and 5.0 V at zero d.c. bias voltage were shown in Fig. 4. The Au/$Y_3N@[C_{80}]^{6-}$/Au structure and its equivalent circuit were shown in the inset of the figure. The

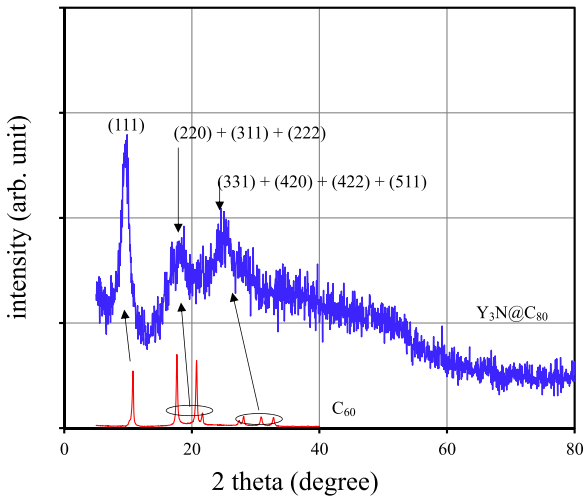

FIG. 3. X-ray diffraction patterns of the as-received $Y_3N@C_{80}$ and C_{60} powder.

Cole – Cole plots are almost linear and perpendicular to Re[Z] axis. From these results, we can conclude that the $Y_3N@[C_{80}]^{6-}$ sample has a small capacitance C_B and an Ohmic contact with the Au electrodes. Therefore, we can ignore the contact resistance from the electrodes and obtain directly the *i-v* characteristics of the $Y_3N@[C_{80}]^{6-}$ sample.

A. Field and temperature-dependent mobility of charge carrier

1. Field and temperature-dependent mobility

The currents at the d.c. bias voltages of 0.5, 1.0, 1.5, 2.0, 3.0, 5.0, 6.0, 10.0, 20.0, 50.0, and 100.0 V during cooling down process were shown in Fig. 5 as a function of reciprocal temperature. The current increases with increasing temperature and no significant difference between cooling down and heating up processes has been observed. It is clear in the figure that the temperature dependences are quite different as two groups, depending on the d.c. bias voltage. When the d.c. bias voltage is above 10.0 V, resistance of the sample

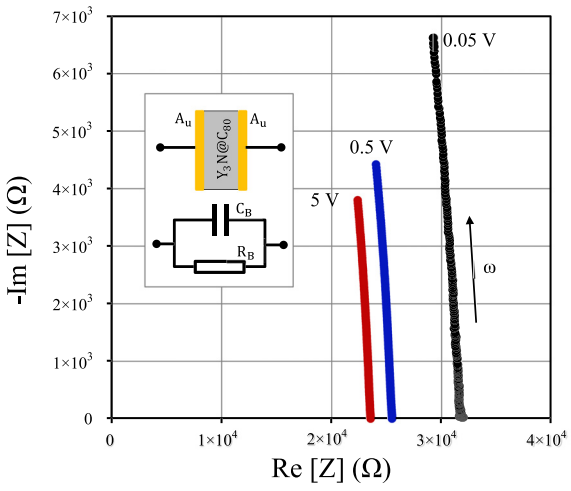

FIG. 4. Cole-Cole plots of impedance of the Au/$Y_3N@[C_{80}]^{6-}$/Au structure at room temperature at the a.c. voltage of 0.05, 0.5, and 5.0 V at zero d.c. bias voltage.

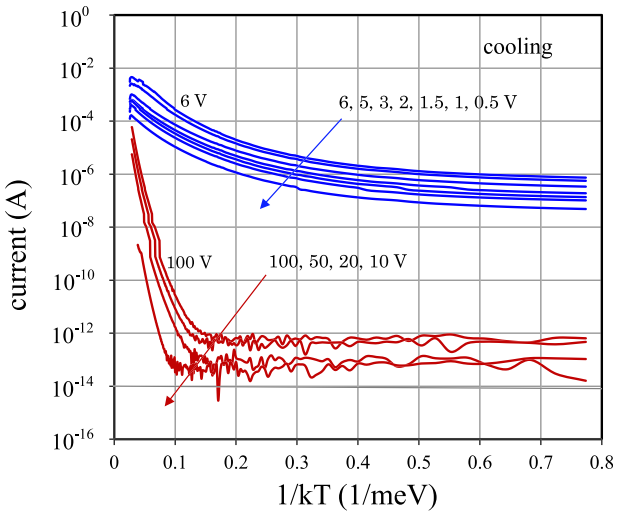

FIG. 5. The current passing through the sample at the d.c. bias voltages of 0.5, 1.0, 1.5, 2.0, 3.0, 5.0, 6.0, 10.0, 20.0, 50.0, and 100.0 V during cooling down process as a function of reciprocal temperature.

increases rapidly and exceeds the limit of the current measurement at temperatures below 80 K, $1/\mathrm{kT} \approx 0.15\ (\mathrm{meV})^{-1}$. The temperature dependences in this group suggest that there are various thermal activation energies for charge carrier transport at various d.c. bias voltages, namely, the mobility of charge carrier depends on both the applied electric field and temperature.

In general, when carrier transport is governed by space charge limited conduction (SCLC) mechanism,[27,28] the i is represented by

$$i(E, T) = \frac{9S\varepsilon_r\varepsilon_0\mu(E, T)E^2}{8L}, \tag{1}$$

where E is the strength of the applied electric field, T is the absolute temperature, S is the area of the electrode, L is the thickness of the sample, $\varepsilon_r\varepsilon_0$ is the permittivity, and $\mu(E, T)$ is the mobility of the charge carrier. Namely, the i is a quadratic function of the electric field $E = v/L$ if the $\mu(E, T)$ is independent of the field. Usually, the mobility $\mu(E, T)$ is field and temperature dependent and is described as follows:[29]

$$\mu(E, T) = \left[\frac{qR^2\nu}{\mathrm{k}T}\right]\exp\left\{-\frac{\epsilon_a - \Delta\epsilon_a}{\mathrm{k}T}\right\}, \tag{2}$$

where R is the distance between nearest-neighbor molecules, ν is the thermal vibration frequency of the host molecule, q is the unit of electronic charge, ϵ_a is the activation energy of the trapped charge carrier, and $\Delta\epsilon_a = (E/4\pi\varepsilon_r\varepsilon_0 q)^{1/2}$ is the change of ϵ_a after the electric field E is applied. Here, $\varepsilon_r\varepsilon_0 = \varepsilon_\infty\varepsilon_0$ is the permittivity at high frequency. For the SCLC mechanism, the mobility of charge carrier depends on both the applied electric field and temperature. One can notice from Eq. (2) that ν is dependent of temperature. Therefore, Eq. (2) can be written as follows:

$$\mu(E, T) = T^\alpha \exp\left\{-\frac{\epsilon_a - \Delta\epsilon_a}{\mathrm{k}T}\right\}, \tag{3}$$

where α is a constant depending on scattering mechanism of the charge carrier during transport.

2. Activation energy of charge carrier

In the case of the d.c. bias voltages below 10.0 V, Arrhenius plots of $(i/T^\alpha) \sim 1/\mathrm{k}T$ at 0.01, 1.0, and 6.0 V during cooling down process were shown in Fig. 6(a). The i increases with temperature in the range of 15–450 K and cannot been fitted using a single exponential function. There are two linear regions in these Arrhenius plots, high temperature region of 300 − 400 K, and low temperature region of 120 − 250 K. There are also different α and ϵ_a at high and low temperature regions as seen from these linear relationships of $i/T^\alpha \sim 1/\mathrm{k}T$ curves. We have conformed from these Arrhenius plots that the i can be fitted by using $\alpha = -1.5$ for high temperature region and $\alpha = 1.5$ for low temperature region, respectively.

Good linear relationships in the Arrhenius plots indicate that electrical transport properties of the $Y_3N@[C_{80}]^{6-}$ sample can be explained using Poole-Frenkel model.[29] The $\alpha = -1.5$ in high temperature region and $\alpha = 1.5$ in low

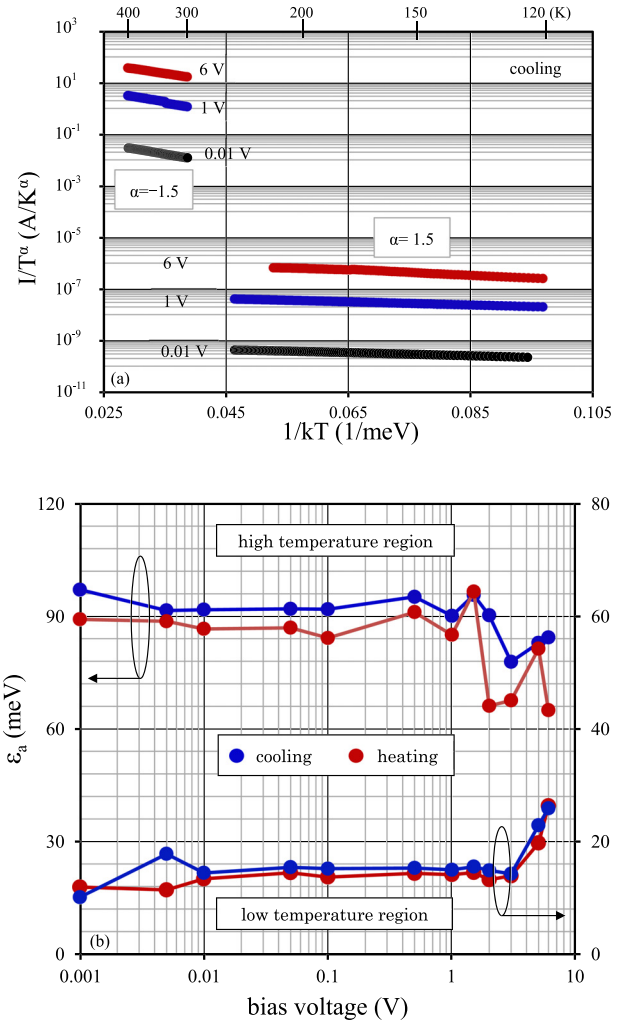

FIG. 6. (a) Arrhenius plots of $(i/T^\alpha) \sim 1/\mathrm{k}T$ at the d.c. bias voltages of 0.01, 1.0, and 6.0 V during cooling down process and (b) activation energies, ϵ_a, in high and low temperature regions during cooling down and heating up processes as a function of d.c. bias voltage.

temperature region suggest various scattering mechanisms of the charge carrier. In high temperature region, phonon scattering is a dominant process, corresponding to $\alpha = -1.5$. On the other hand, ion scattering is a major process in low temperature region, corresponding to $\alpha = 1.5$. These properties are similar to the transport of charge carrier in normal semiconductors such as Si and Ge crystals.

From Arrhenius plots in Fig. 6(a), we obtained the activation energies of the trapped charge carrier to excite to the conducting states. The activation energies, ϵ_a, in high and low temperature regions during cooling down and heating up processes were shown in Fig. 6(b) as a function of the d.c. bias voltage. In high temperature region, the activation energy is almost constant, about 88.7 meV at the d.c. bias voltages below 2.0 V. But, it decreases somewhat when the d.c. bias voltage is above 2.0 V. On the other hand, the activation energy is also constant, about 13.6 meV, and increases when the d.c. bias voltage is above 2.0 V. The $\Delta\epsilon_a$ is very small and can be ignored as compared with ϵ_a.

In the case of the d.c. bias voltages above 10.0 V, we observed an interesting transport property of the $Y_3N@[C_{80}]^{6-}$ sample for the first time that ion scattering is a dominant process over the temperature range of $100 - 450$ K. This is quite different from the case at the d.c. bias voltages below 10.0 V as shown in Figs. 5 and 6(a). Arrhenius plots of $(i/T^{\alpha}) \sim 1/kT$ at the d.c. bias voltages of 10.0 V, 50.0 V, and 100.0 V during cooling down process were drawn in Fig. 7(a). Linear $(i/T^{\alpha}) \sim 1/kT$ curves with different α and ϵ_a in high temperature region of $270 - 400$ K and low temperature region of $120 - 220$ K were observed. The i can be fitted using $\alpha = 0.5$ or high temperature region and $\alpha = 1.0$ for low temperature region, respectively. Those positive values of $\alpha = 0.5$ and 1.0 indicate a dominant ion scattering mechanism during charge carrier transport. The results also suggest that there is an order phase transition of the dipole on the Y_3N cluster inside the C_{80} cage under high electric fields in temperature range of $100 - 450$ K because ionic scattering is always beyond lattice scattering. The α values in Fig. 6(a), $\alpha = -1.5$ in high temperature region and $\alpha = 1.5$ in low temperature region, indicate that the effects of $Y_3N@[C_{80}]^{6-}$ anions on carrier transport can be ignored when the Y_3N cluster dipoles are on a disorder distribution under low electric fields. On the other hand, when the Y_3N cluster dipoles are on an order distribution under high electric fields as shown in Fig. 7(a), ionic scattering is beyond lattice scattering due to a long-range ordered array of the Y_3N cluster dipoles.

The activation energies in high and low temperature regions during cooling down and heating up processes were shown in Fig. 7(b) as a function of the d.c. bias voltage. The activation energy in high temperature region decreases with increasing the d.c. bias voltage and reaches to a constant value of 288.5 meV at 100.0 V. On the other hand, the activation energy in low temperature region also decreases with increasing the d.c. bias voltage and reaches to a constant value of 146.5 meV at 100.0 V. Compared with the sample under low electric field, the charge carriers are difficult to freely move in this anionic solid due to larger activation energies.

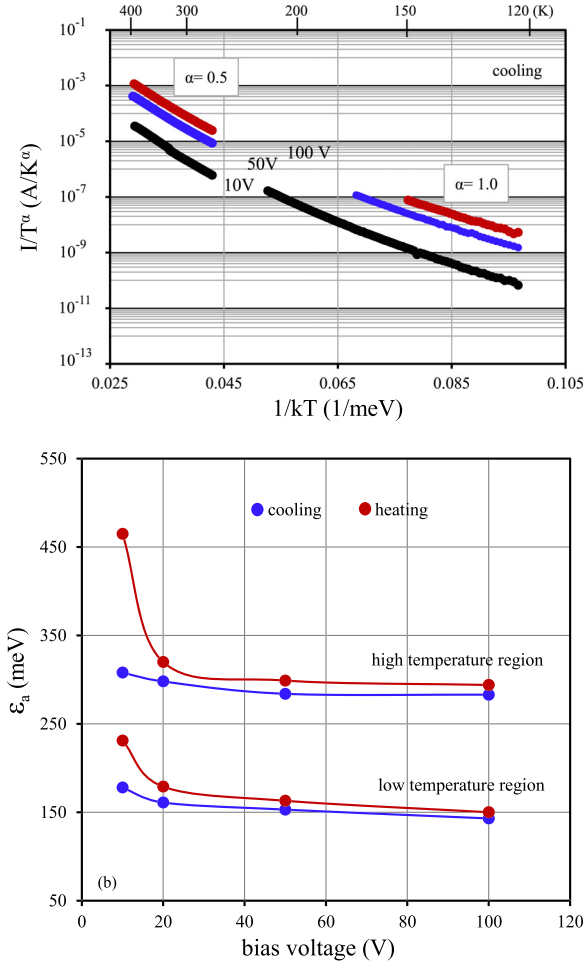

FIG. 7. (a) Arrhenius plots of $(i/T^{\alpha}) \sim 1/kT$ at the d.c. bias voltages of 10.0, 50.0, and 100.0 V during cooling down process and (b) activation energies, ϵ_a, in high and low temperature regions during cooling down and heating up processes as a function of d.c. bias voltage.

B. Field-induced order phase transition of Y_3N cluster

1. Field-dependent distance between $Y_3N@[C_{80}]^{6-}$ anions

The i-v characteristics of the $Au/Y_3N@[C_{80}]^{6-}/Au$ structure at temperatures of 100, 300, and 400 K were shown in Fig. 8. In the temperature range of $100 - 400$ K, the current passing through the sample is strongly dependent of the d.c. bias voltage or the electric field E in the sample. There are three unique regions on the i-v characteristics at temperatures of 100, 300, and 400 K. First, at the d.c. bias voltages below 2.0 V, the current can be fitted as a quadratic function of the d.c. bias voltage. The quadratic i-v characteristic is similar to a hopping conductance of charge carrier in molecular materials[30] and is distinctly different to an exponential i-v characteristic of the Schottky barrier or a linear i-v characteristic of metal. Second, at the d.c. bias voltages ranged from 2.0 to 6.0 V, the current was fitted as a quartic function of the d.c. bias voltage. Third, the current decreased discontinuously and can be fitted as a quadratic function of the d.c. bias voltage when it was above 10.0 V.

As showed in Eq. (1), the current is a quadratic function of the d.c. bias voltage if the mobility $\mu(E, T)$ is

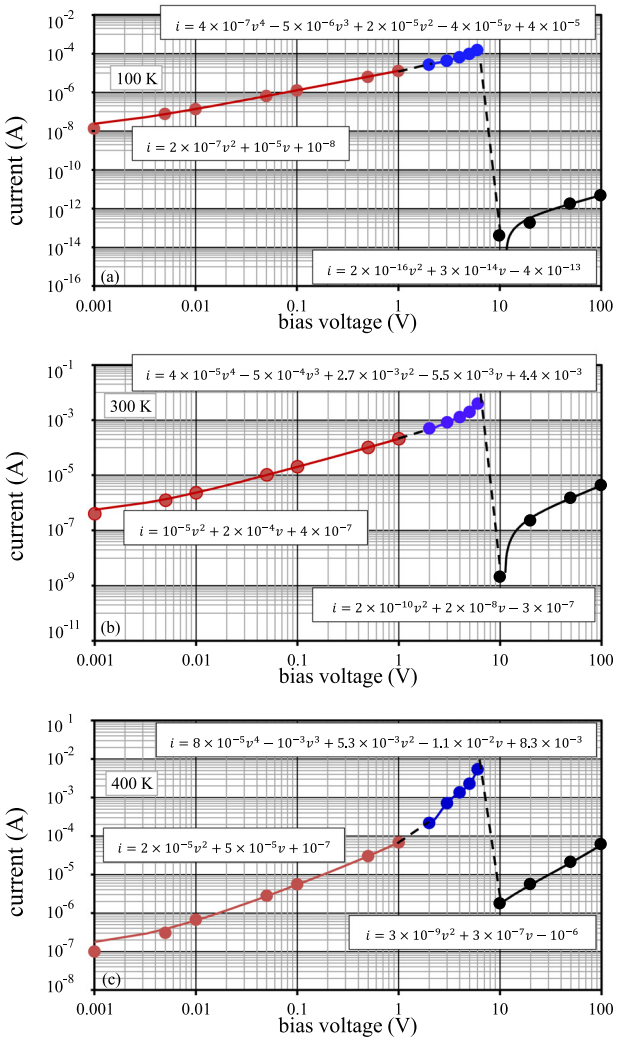

FIG. 8. The *i-v* characteristics of the $Y_3N@[C_{80}]^{6-}$ anionic solid sample at temperatures of (a) 100 K, (b) 300 K, and (c) 400 K.

independent of the electric field *E*. This is consistent with our results measured at the d.c. bias voltages below 2.0 V. It has been reported already that there is a charge transfer between the Y_3N cluster and the C_{80} carbon cage. As a result of the charge transfer, six electrons moved to the C_{80} cage and led to that all $Y_3N@C_{80}$ molecules become to $Y_3N@[C_{80}]^{6-}$ anions in the sample. In the $Y_3N@[C_{80}]^{6-}$ solid phase, the anion density is the same with molecular density, and the mean free pass of the charge carrier is comparable to the intermolecular distance, *R*. One can notice from Eqs. (1) and (2) that the *i-v* characteristics become to a quartic function of the d.c. bias voltage, if the *R* is proportional to the applied electric field *E*. In fact, the ionic radius of Y^{3+} (1.01 Å) is larger than that of Sc^{3+} (0.87 Å) and Lu^{3+} (1.00 Å). Thus, the Y_3N cluster in the C_{80} cage has a pyramid form while the Sc_3N and Lu_3N clusters have a plane form.[8,31] This asymmetric structure of the pyramid cluster unit results in a dipole **δ** which points from N^- to Y^+ as shown in Fig. 9. The dipole **δ** results in an attractive force between the clusters, so that, between the $Y_3N@[C_{80}]^{6-}$ anions under the applied electric field. If change of the *R* due to the *E* is small, we have

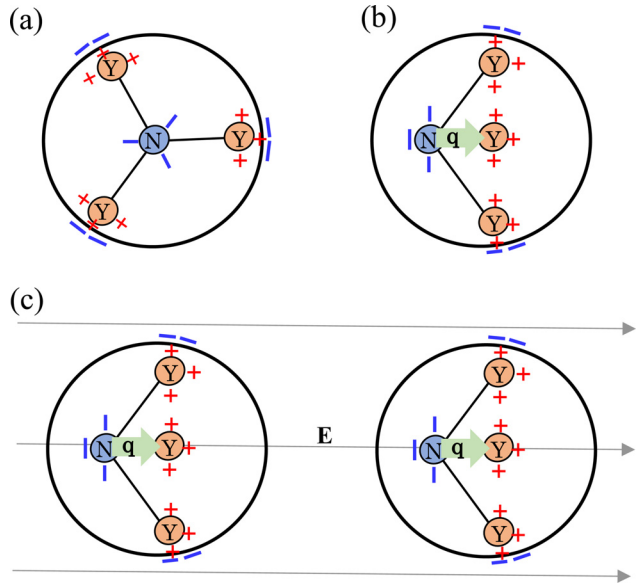

FIG. 9. Diagrams of the $Y_3N@[C_{80}]^{6-}$ anion. (a) Top view, (b) side view, and (c) side view under an electric field.

$$R(E) = \sum_{0}^{\infty} \frac{R(E_0)^{(n)}}{n!}(E - E_0)^n \approx A + B(E - E_0), \qquad (4)$$

where A and B are constant. Therefore, we obtained from Eqs. (1) and (2) that the *i-v* characteristic is a quadratic function of the d.c. bias voltage when the *R* is independent of the *E*. On the other hand, the characteristic is a quartic function if there is a linear relationship between the *R* and *E*.

At the d.c. bias voltages above 10.0 V, a new order phase appears because resistance of the anion solid increases over three orders of magnitude at temperatures of 100, 300, and 400 K as seen in Fig. 8. In the new order phase under high electric fields, the mobility of charge carrier may be independent of the field *E* because the anions are on the equilibrium positions in the new order phase. Therefore, the current becomes a quadratic function of the d.c. bias voltage again. In order to clarify mechanisms of the order phase transition, further studies using other measurement techniques are necessary.

We also must point out that there are free charge carriers of a small amount in the sample at temperatures below 100 K while the trapped carriers with activation energies of 13.6, 88.7, 146.5, and 288.5 meV cannot be completely excited. The *i-v* characteristics of the $Y_3N@[C_{80}]^{6-}$ anionic sample around 100 K were listed in Table I. On the *i-v*

TABLE I. The *i-v* characteristics of the $Y_3N@[C_{80}]^{6-}$ anionic sample around the temperature of 100 K.

Temperature (K)	*i-v* characteristics
110	$i = 3\times10^{-6}v^2 + 2\times10^{-5}v + 7\times10^{-8}$
105	$i = 3\times10^{-6}v^2 + 1\times10^{-5}v + 6\times10^{-8}$
100	$i = 2\times10^{-7}v^2 + 1\times10^{-5}v + 1\times10^{-8}$
99	$i = 1\times10^{-5}v^{1.00}$
95	$i = 1\times10^{-5}v^{1.00}$
90	$i = 1\times10^{-5}v^{0.98}$

characteristics of $i = av^2 + bv + c$, the constants of a and c become small and b is constant with decreasing temperature in the narrow temperature range. In Table I, it is clear that the i-v characteristic can be fitted by $i = av^2 + bv + c$ for temperatures above 100 K and by a linear function of $i = bv$ for temperatures below 100 K at the biases below 1.0 V. The result suggests that the $Y_3N@[C_{80}]^{6-}$ anion sample is a conductor with a constant conductance of $b = i/v$ at temperatures below 100 K. On the other hand, at temperatures below 100 K and the biases ranged from 1.5 to 10.0 V, the i-v characteristic is a quartic function of $i = av^4 + bv^3 + cv^2 + dv + e$, which is consistent with the results in Fig. 8. The i-v characteristic at 15 K, a linear relationship between the current and the d.c. bias voltage, was shown in Fig. 10.

2. Cluster dipole effect

As seen in Figs. 8 and 10, the order phase transition appears in wide temperature range from 15 to 450 K and only depends on the applied electric field. This result suggests that the phase transition is not a thermal activation process. For example, an order-disorder phase transition associated with molecular rotation with activation energy of 35 ± 15 meV appears in the C_{60} crystal at 260 K.[32] If the transition observed in this study is associated with rotation of the $Y_3N@C_{80}$ molecules, an activation energy larger than that of the C_{60} rotation is necessary because of large molecular radius of the C_{80} cage. Theoretical calculations have showed that activation energy of the rotation of the Y_3N cluster in the C_{80} cage is 122.0 meV.[21] Therefore, at low temperatures below 300 K, thermal rotation of the Y_3N cluster will be frozen because of thermal energies below 25.9 meV. Also, the dipole $\boldsymbol{\delta}$ cannot be completely screened by electrons on the C_{80} cage due to large activation energies as shown in Figs. 6(b) and 7(b). Based on the above results, we can conclude that the order phase transition in the $Y_3N@[C_{80}]^{6-}$ anion solid is associated with the Y_3N cluster dipole $\boldsymbol{\delta}$ under the applied electric field. The rotation moment $\boldsymbol{N} = \boldsymbol{\delta} \times \boldsymbol{E}$ of the Y_3N cluster may overcome the friction between the cluster and the C_{80} cage at higher electric field strengths. Using the data about the pyramidal structure of Y_3N cluster in the C_{80} cage,[31] we obtained the maximum rotation moment of Y_3N cluster, 1.25×10^{-22} N · cm^{-1}.

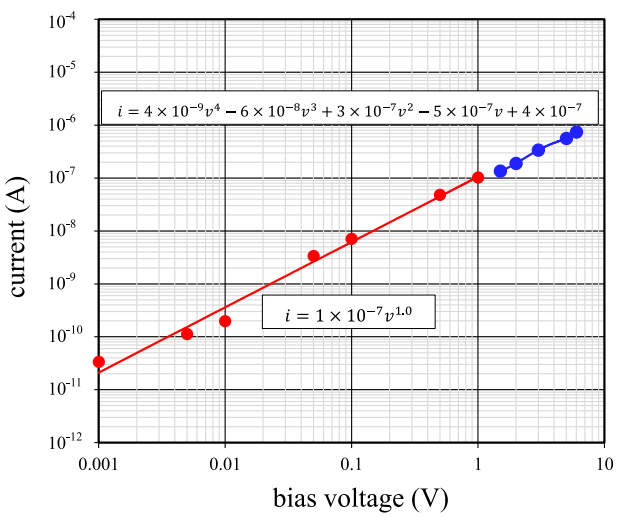

FIG. 10. The i-v characteristic of the $Y_3N@[C_{80}]^{6-}$ anionic solid sample at 15 K.

3. Dimerization effect

The endohedral fullerenes have a tendency to form dimers especially in solid state. The dimerization has been explained by intermolecular interactions originating from a permanent dipole moment or an unpaired electron at the fullerene cage.[33,34] Recently, a dimerization effect of the $M_3N@C_{80}$ molecules was reported that dianionic dimers were formed when two $M_3N@C_{80}$ molecules get one electron each.[35,36] The dimers result in chemical bond which decreases molecular distance, as compared with that in van der Waals solid. The dimerization leads to a structural rearrangement of the $M_3N@C_{80}$ anions.[36] Also, the $M_3N@C_{80}$ anions are more prone to dimerization and are substantially more stable than their empty anions.

Superatom molecular orbitals (SAMOs) in the $Sc_3N@C_{80}$ have been observed by using scanning tunneling microscopy and spectroscopy.[37] The Sc_3N cluster in $Sc_3N@C_{80}$ distorts the nearly-spherical central potential of the carbon cage, imparting an asymmetric spatial distribution to the SAMOs. When $Sc_3N@C_{80}$ molecules form dimers or trimers, the strong intermolecular hybridization results in highly symmetric SAMOs with clear bonding and antibonding characteristics.

It is possible that the distance between the $Y_3N@[C_{80}]^{6-}$ anions decreases when electrons are supplied into the anion solid sample due to the effects of the cluster dipole and superatom, which result in the field-dependent carrier mobility.

C. Ohmic resistance of the $Y_3N@[C_{80}]^{6-}$ anionic solid

An understanding of dielectric properties is very important to clarify the carrier transport and lattice polarization mechanisms of the anionic solid sample. We have measured dielectric constant of the $Y_3N@[C_{80}]^{6-}$ anion sample at the a.c. magnitudes from 0.01 V to 5.0 V. The relative permittivities at room temperature at the a.c. magnitudes of 0.05 V, 0.5 V, and 5.0 V were shown in Fig. 11 as a function of frequency. No significant a.c. magnitude dependence was observed. The relative permittivity, ε_r, decreases with increasing frequency due to a relaxation time $\tau = C_B R_B$,[26,38] where C_B and R_B depend on frequency as shown in Fig. 4. The relative permittivitiy has a value of 828 at 1.0 MHz, which is much larger than 34.0 of the $Sc_3N@C_{80}$ at frequencies above 100 Hz (Ref. 39) and 4.6 of $Er_3N@C_{80}$ at frequency of 5 MHz.[26] This large permittivity is related to the free moving charges which results in an Ohmic resistance on the $Y_3N@[C_{80}]^{6-}$ anion sample. As shown in Fig. 10, the free moving charges were observed at temperatures below 15 K, which may correspond to an activation energy below ~2.0 meV.

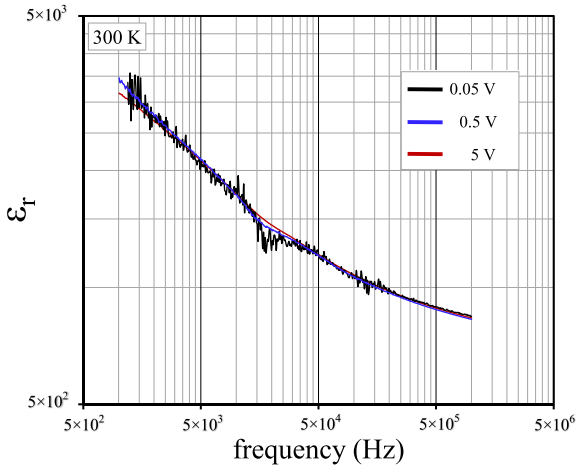

FIG. 11. Relative permittivities of the $Y_3N@[C_{80}]^{6-}$ anionic solid sample at room temperature at the a.c. magnitudes of 0.05, 0.5, and 5.0 V as a function of frequency.

The impedance of the $Y_3N@[C_{80}]^{6-}$ anion sample for a parallel combination of the bulk capacitance C_B and resistance R_B can be written as follows:

$$Z(\omega) = \frac{R_B}{1+\omega^2 C_B^2 R_B^2} - j\omega \frac{C_B R_B^2}{1+\omega^2 C_B^2 R_B^2}. \quad (5)$$

From Eq. (5), we have the equivalent capacitance, C',

$$C' = \frac{1+\omega^2 C_B^2 R_B^2}{\omega^2 C_B R_B^2}. \quad (6)$$

When $R_B \to \infty$, we have $C' = C_B$, and when $R_B \to 0$, $C' \to \infty$. Therefore, the C', measured in this study, decreases with increasing frequency and have a larger equivalent capacitance if $R_B \neq 0$. This C' results in a large ε_r due to presence of the bulk resistance R_B. We can obtain the true value of ε_r when $\omega \to \infty$ only.

Based on the results above, we obtained that both the *i-v* characteristics of the anion sample and the activation energies of the charge carriers in the sample depend on temperature and the applied electric field. The *i-v* characteristics were listed in Table II. At the temperatures below 100 K and the field strengths below 30 Vcm^{-1}, an Ohmic resistance, $i \propto v$, is observed. With increasing temperature, the i becomes to a function of v^2. This characteristic indicates that mobility of the charge carrier is independent of electric field. When the electric field is beyond 30 Vcm^{-1}, the i is a function of v^4 for which the mobility is a quadratic function of the field. At the field strengths above 120 Vcm^{-1}, the i becomes to a function of v^2 again. This relationship corresponds to a new order phase induced under high electric fields.

TABLE II. The *i-v* characteristics of the $Y_3N@[C_{80}]^{6-}$ anionic sample at various temperatures and field strengths. The O.R. means over range of digital electrometer during the current measurement.

T(K) / E(Vcm^{-1})	15–100	100–250	250–450
0–30	$i \propto v$	$i \propto v^2$	$i \propto v^2$
30–120	$i \propto v^4$	$i \propto v^4$	$i \propto v^4$
120–2000	O.R.	$i \propto v^2$	$i \propto v^2$

TABLE III. Activation energies of the carrier mobility of the $Y_3N@[C_{80}]^{6-}$ anionic sample at various temperatures and field strengths, in the unit of meV. The O.R. means over range of digital electrometer during the current measurement.

T(K) / E(Vcm^{-1})	15–100	100–250	250–450
0–30	NO	13.6	88.7
30–120	O.R.	146.5	288.5
120–2000	O.R.	O.R.	O.R.

The activation energies of the carrier mobility were listed in Table III in the unit of meV. At the temperatures below 100 K and the field strengths below 30 Vcm^{-1}, Ohmic resistance was observed. At high temperatures above 100 K, a thermally activated mobility was observed in the anion sample.

IV. CONCLUSION

The *i-v* characteristics of the $Y_3N@[C_{80}]^{6-}$ anionic solid were measured at various temperatures and electric fields. Four conducting phases were observed in this anionic solid. These conducting phases correspond to Ohmic conduction, space charge limited conduction, field-dependent intermolecular distance conduction, and Y_3N cluster high-ordered phase conduction in the anionic solid. First, at temperatures below 100 K and field strengths below 30 Vcm^{-1}, the current passing through the anionic solid was a linear function of the d.c. bias voltage, namely, a constant conductance due to free moving charges. Second, at the same field strengths, the trapped carrier was thermally activated with activation energies of 13.6 meV for the temperature range of 100 – 250 K and 88.7 meV for 250 – 450 K. The activation energies were independent of electric field strength. In this conducting phase, the carrier transport was governed by space charge limited conduction mechanism. Third, when the applied electric field increased from 30 to 120 Vcm^{-1}, the current became a quartic function of the field strength. This *i-v* relationship indicates that the carrier mobility is a quadratic function of the field strength or a linear relationship between the nearest-neighbor anion distance and electric field strength. A conducting phase with high resistance appeared at temperatures below 100 K, and the trapped carrier was thermally activated with activation energies of 146.5 meV for the temperature range of 100 – 250 K and 288.5 meV for 250 – 450 K. Finally, at the electric field strengths of 120 – 2000 Vcm^{-1}, an order phase transition of the Y_3N cluster inside the C_{80} cage in the anionic solid at temperatures below 100 K appeared and results in high resistance. In this conducting phase with the ordered structure of the Y_3N cluster, the current was a quadratic function of the d.c. bias voltage, and the carrier mobility was independent of the field strength.

Electrical transport properties of the anionic solid were very sensitive to the applied electric field due to an ordering effect of dipole on the Y_3N cluster inside the C_{80} cage. The field-sensitive properties were also related to a low screening effect of free moving carriers in the solid because of both large activation energy and small mobility.

ACKNOWLEDGMENTS

This work was partially supported by project No. 15-B01, Program of Research for the Promotion of Technological Seeds, Japan Science and Technology Agency (JST). The work was also partially supported by Grant-in-Aid for Exploratory Research No: 23651115, Japan Society for the Promotion of Science (JSPS).

[1]J. Park, A. N. Pasupathy, J. I. Goldsmith, C. Chang, Y. Yaish, J. R. Petta, M. Rinkoski, J. P. Sethna, H. D. Abruna, P. L. McEuen, and D. C. Ralph, Nature **417**, 722 (2002).
[2]T. I. Smirnova, A. I. Smirnov, T. G. Chadwick, and K. L. Walker, Chem. Phys. Lett. **453**, 233 (2008).
[3]E. Xenogiannopoulou, S. Couris, E. Koudoumas, N. Tagmatarchis, T. Inoue, and H. Shinohara, Chem. Phys. Lett. **394**, 14 (2004).
[4]D. W. Cagle, T. P. Thrash, M. Alford, L. P. F. Chibante, G. J. Ehrhardt, and L. J. Wilson, J. Am. Chem. Soc. **118**, 8043 (1996).
[5]S. Sato, S. Seki, G. Luo, M. Suzuki, J. Lu, S. Nagase, and T. Akasaka, J. Am. Chem. Soc. **134**, 11681 (2012).
[6]O. Tishchenko and D. G. Truhlar, J. Phys. Chem. Lett. **4**, 422 (2013).
[7]S. Y. Yang, M. Yoon, C. Hicke, Z. Y. Zhang, and E. Wang, Phys. Rev. B **78**, 115435 (2008).
[8]S. Stevenson, G. Rice, T. Glass, K. Harich, F. Cromer, M. R. Jordan, J. Craft, E. Hadju, R. Bible, M. M. Olmstead, K. Maitra, A. J. Fisher, A. L. Balch, and H. C. Dorn, Nature **401**, 55 (1999).
[9]H. Shinohara, Rep. Prog. Phys. **63**, 843 (2000).
[10]L. Dunsch and S. Yang, Small **3**, 1298 (2007).
[11]I. N. Ioffe, A. S. Ievlev, O. V. Boltalina, L. N. Sidorov, H. C. Dorn, S. Stevenson, and G. Rice, Int. J. Mass Spectrom. **213**, 183 (2002).
[12]X. Lu, T. Akasaka, and S. Nagase, Chem. Commun. **47**, 5942 (2011).
[13]J. He, K. Wu, R. Sa, Q. Li, and Y. Wei, Chem. Phys. Lett. **475**, 73 (2009).
[14]A. Mayer, Ph. Lambin, and R. Langlet, Appl. Phys. Lett. **89**, 063117 (2006).
[15]A. Mayer, Ph. Lambin, and P.-O. Åstrand, Nanotechnology **19**, 025203 (2008).
[16]C. M. Cardona, A. Kitaygorodskiy, A. Ortiz, M. Á. Herranz, and L. Echegoyen, J. Org. Chem. **70**, 5092 (2005).
[17]T. Cai, Z. Ge, E. B. Iezzi, T. E. Glass, K. Harich, H. W. Gibson, and H. C. Dorn, Chem. Commun. **28**, 3594 (2005).
[18]C. M. Cardona, A. Kitaygorodskiy, and L. Echegoyen, J. Am. Chem. Soc. **127**, 10448 (2005).
[19]S. Osuna, R. Valencia, A. Rodriguez-Fortea, M. Swart, M. Sola, and J. M. Poblet, Chem. Eur. J. **18**, 8944 (2012).
[20]W. Fu, L. Xu, H. Azuremendi, J. Ge, T. Fuhrer, T. Zuo, J. Reid, C. Shu, K. Harich, and H. C. Dorn, J. Am. Chem. Soc. **131**, 11762 (2009).
[21]W. Fu, X. Wang, H. Azuremendi, J. Zhang, and H. C. Dorn, Chem. Commun. **47**, 3858 (2011).
[22]L. H. Gan and R. Yuan, Chem. Phys. Chem. **7**, 1306 (2006).
[23]T. Takase, M. Sakaino, K. Kirimoto, and Y. Sun, Appl. Phys. A **112**, 927 (2012).
[24]Y. Sun, Y. Hattori, M. Sakaino, F. Morimoto, and K. Kirimoto, Mater. Sci. Appl. **4**, 808 (2013).
[25]Y. Sun, K. Kirimoto, M. Sakaino, and F. Morimoto, Jpn. J. Appl. Phys., Part 1 **53**, 035102 (2014).
[26]Y. Sun, Y. Maeda, H. Sezaimaru, M. Sakaino, and K. Kirimoto, J. Appl. Phys. **116**, 034301 (2014).
[27]D. H. Dunlap, P. E. Parris, and V. M. Kenkre, Phys. Rev. Lett. **77**, 542 (1996).
[28]M. A. Lampert and P. Mark, *Current Injection in Solids* (Academic Press, New York, 1970), p. 27.
[29]J. G. Simmons, Phys. Rev. **155**, 657 (1967).
[30]N. Karl, Synth. Met. **133–134**, 649 (2003).
[31]L. Echegoyen, C. J. Chancellor, C. M. Cardona, B. Elliott, J. Rivera, M. M. Olmstead, and A. L. Balch, Chem. Commun. **25**, 2653 (2006).
[32]D. A. Neumann, J. R. D. Copley, R. L. Cappelletti, W. A. Kamitakahara, R. M. Lindstrom, K. M. Creegan, D. M. Cox, W. J. Romanow, N. Coustel, J. P. Mccauley, N. C. Maliszewskyj, J. E. Fischer, and A. B. Smith, Phys. Rev. Lett. **67**, 3808 (1991).
[33]N. Lin, H. J. Huang, S. H. Yang, and N. Cue, Phys. Rev. B **58**, 2126 (1998).
[34]Y. Hasegawa, Y. Ling, S. Yamazaki, H. Shinohara, A. Sakai, H. W. Pickering, and T. Sakurai, Phys. Rev. B **56**, 6470 (1997).
[35]A. A. Popov, S. M. Avdoshenko, G. Cuniberti, and L. Dunsch, J. Phys. Chem. Lett. **2**, 1592 (2011).
[36]S. Yang, M. Zalibera, P. Rapta, and L. Dunsch, Chem. Eur. J. **12**, 7848 (2006).
[37]T. Huang, J. Zhao, M. Feng, H. Petek, S. Yang, and L. Dunsch, Phys. Rev. B **81**, 085434 (2010).
[38]M. Sakaino, Y. Sun, and F. Morimoto, J. Appl. Phys. **115**, 023701 (2014).
[39]H. M. Ahmed, M. K. Hassan, K. A. Mauritz, S. L. Bunkley, R. K. Buchanan, and J. P. Buchanan, J. Appl. Polym. Sci. **131**, 40577 (2014).